Benha Journal of Applied Sciences (BJAS) **print: ISSN 2356–9751**
Vol.(5) Issue(7) Part (2) (2020), (199-208) **online: ISSN 2356–976x**
http://bjas.journals.ekb.eg

Sol-Gel Auto-Combustion Preparation and Characterization of Silica Nanoparticles for The Removal of Congo Red Dye from Aqueous Media

A. A. Ali, H. M. Aly, I. S. Ahmed, and F. M. Fathi
Chemistry Department, Faculty of Science, Benha University, Benha, Egypt
E-Mail**:** ayman.abdelrazik@fsc.bu.edu.eg

Abstract

Silica nanoparticles have been successfully synthesized by a modified sol-gel auto combustion synthesis method using silica gel and PEG 4000. The as-prepared silica was calcined at 800 ºC for 4 h following by the characterization using various tools such as XRD, FT-IR, and FE-SEM. The average crystallite size of the calcined Silica was determined to be 3-7.5 nm. FTIR spectroscopy confirmed the presence of a silica sample according to the presence of the peaks at 468, 665, 811, and 1064 cm^{-1}. The FE-SEM photograph displayed that the calcined silica nanoparticles are agglomerated in spherical shapes and the average agglomerated particle size in the range of 91 nm. The batch adsorption was applied for the removal of congo red dye over the fabricated silicon oxide adsorbent under various experimental conditions. The extracted adsorption data applied for the investigation of adsorption isotherm and kinetic models. Also, the thermodynamic parameters were examined for the removal of congo red dye over silicon oxide nanoparticles.

Keywords: Silica nanoparticles; Sol-gel auto-combustion method; Calcination; Congo red dye

1. Introduction

Silica nanoparticles prepared by using various techniques such as microwave [1] and sol-gel [2] methods. These methods have different effects of the synthesized material such as particle size, shape, formation time, morphology, etc. [3]. The synthesis of silica with PEI based on the doped polyethyleneimine (PEI) inside silica nanoparticles to get the (PEI) silica nanoparticles [4]. The preparation method can be used CTAB to form mesostructured silica cores [5, 6]. it also synthesized hollow mesoporous silicate particles with minimum structural defects [7]. Silica nanoparticles used in different applications such as biomedical (as enzymes and drug delivery) [8-10], high-performance thermal insulation material [11], white cement as a binder [12], fuel cell, electrolyte membrane [13, 14], high-performance matrix for many catalysts [15]. Also, silica nanoparticles showed a good adsorption capacity for the removal of some pollutants from aqueous solutions such as congo red dye [16] and methylene blue dye [17, 18]. Rapid pyrolysis at high temperatures is a promising process to obtain black SiO_2 nanoparticles [19], which can be applied in different areas for its characteristic color such as cosmetics, graphite, paints, ceramics, and polymer industry. It can be used for the removal of some organic compounds.

Amorphous silica nanoparticles with high purity were synthesized using precipitation following by the calcination [20]. Silica nanoparticles adsorbent have may practical applications for the removal of different heavy metals [21-23] such as lead and cadmium from the polluted water [24, 25]. Also, silica nanoparticles were increased the removal capacity of nitrate from water due to an increase in surface positive charges and provision of new surface functional groups [26]. the combustion synthesis method is also known as low solution combustion synthesis and it used for the preparation of simple and complex inorganic compounds [27-31]. In the present work, we aimed to synthesize silica nanoparticles by using the sol-gel auto combustion synthesis method following by the calcination to improve the crystallinity of the synthesized silica. The structure, functional groups, and morphology properties of the obtained silica are characterized by different tools such as XRD, FT-IR, and SEM.

2. Experimental

2.1. Materials and reagents

All chemicals and reagents in this work were of analytical grade and they were purchased and employed as received without further purification. Silica gel (60-120 mesh), Sodium hydroxide (NaOH, 99%), nitric acid (HNO_3, 69%), and polyethylene glycol 4000 (PEG 4000) were purchased from El Nasr pharmaceutical chemicals company.

2.2. Preparation of silica nanoparticles

0.02 mole of silica gel was dissolved in 0.04 mole of sodium hydroxide solution with stirring at 80°C for 10 minutes to complete the solubility of the silica gel. After the solution was cooled, pH of the solution decreases using nitric acid (2M) to obtain the gel (pH= 7). The obtained gel was centrifuged and washed several times with distilled water. 0.1, 0.5, 0.75 grams of polyethylene glycol (4000) was added to the produced gel with 20 ml distilled water with stirring at 80°C for 1h. The obtained gel was dehydrated at 150 °C for 2 h in an electric furnace. The white solid material was auto-ignited at 350 °C on a hot plate. The combustion reaction was

completed in 10 minutes and the grey powder was obtained. The synthesized silica was well ground and calcined at 800 °C for 4 h., to get the crystalline silica nanoparticles. Figure (1) shows a schematic flowchart for the preparation of silicon dioxide using a sol-gel auto combustion method using different weights of PEG. Table 1 outlined the names of products, the ratio between the reactants according to the weight of PEG in the combustion method. The synthesized samples were named by SE18, SE28, and SE38 after calcination at 800 ^{o}C for 4 h.

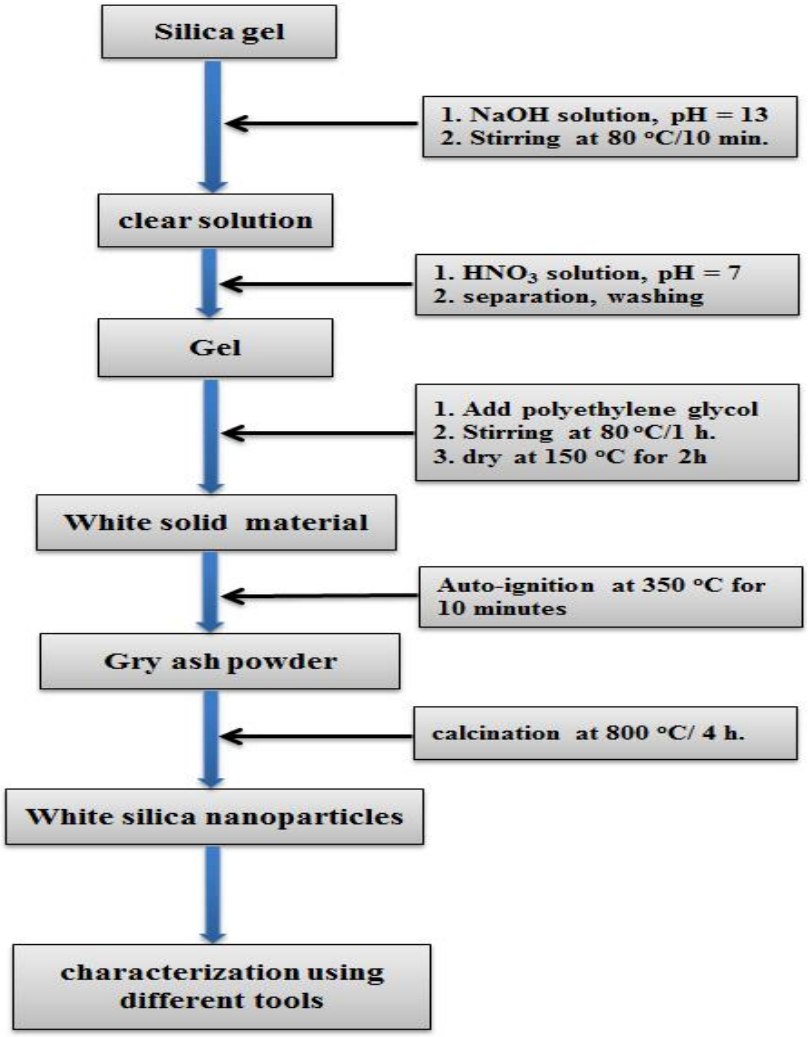

Fig (1): Flowchart of the synthesis of silica nanoparticles.

Table 1
The names of products and the ratio between the reactants in the preparation of silicon oxide

S. name	Silica gel, mole	PEG, g	Si/PEG, wt. ratio
SE18	0.02	0.1	12.0
SE28	0.02	0.5	2.4
SE38	0.02	0.75	1.6

2.3. Characterization:

X-ray diffraction (XRD) of the sample was measured using a diffractometer (Bruker; model D8 advance) with monochromatic Cu-Ka radiation, 1.54178 (˚A) in the 2θ range of 15-80º. FTIR spectra were measured using the FT-IR spectrometer (Bomem; model MB 157S) from 4000 to 400 cm^{-1} at room temperature. The morphology of the prepared sample was studied using a Field emission scanning electron microscope (FE-SEM, JEOL: model JSM-6500F).

3. Result and Discussion

3.1. Characterization of the synthesized silicon oxide

Figure (2) displays the XRD patterns of the calcined silicon dioxide (SE18, SE28, and SE38 samples). The extracted data shows that the pure crystalline silicon oxide nanoparticles were obtained with the diffraction peaks according to XRD card No. 82-1403 and 86-0681 for Cristobalite and Tridymite. From the extracted data of XRD analysis, the effect of PEG appeared on the synthesized silicon oxide phase. The average crystallite sizes of silicon dioxide calculated by using the Debye-Scherrer formula No. (1).

$$X = 0.9\lambda / B_{1/2}\cos\theta \quad (1)$$

Where λ is the wavelength (1.5406 A for CuKα), θ is the diffraction angle and β is the x-ray full width at half maximum height of the diffraction peak. The average crystallite size of the calcined silica (X) is determined to be 3 nm, 3 nm, and 7.5 nm for SE18, SE28, and SE38, respectively.

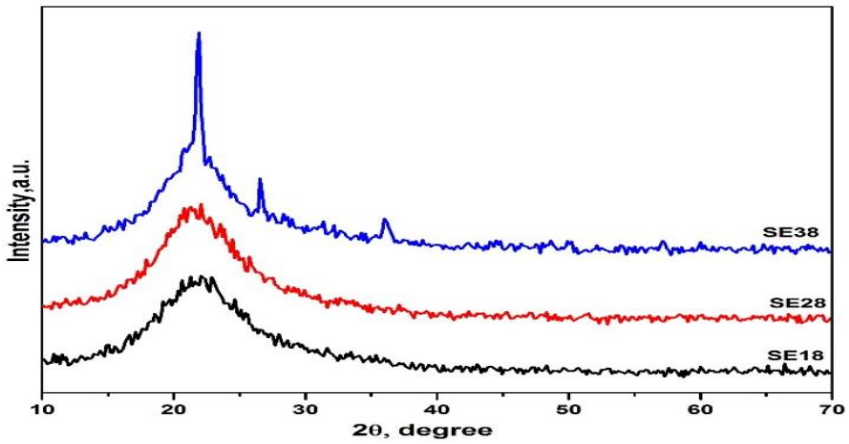

Fig (2): XRD patterns of silica sample after calcination at 800 ºC for 4 h (SE18, SE28, and SE38 samples).

Figure (3) displays the FT-IR spectra of the synthesized silica after calcination at 800 ºC. The two weak and broad bands appeared at 1635 and 3438 cm^{-1} are corresponding to bending and stretching vibrations of the adsorbed -OH groups on the surface nanomaterial. FTIR spectrum showed absorption bands at 468, 665, 811, and 1064 cm^{-1} corresponding to a pure SiO_2 product. The absorption band appeared at 468 cm^{-1} due to the siloxane bond (Si-O-Si) bending vibration. The bands at 665 and 811 cm^{-1} can be attributed to symmetric stretching vibrations of the Si-O-Si bond. While the band observed at 1064 cm^{-1} returned to an asymmetric stretching vibration of the Si-O-Si bond.

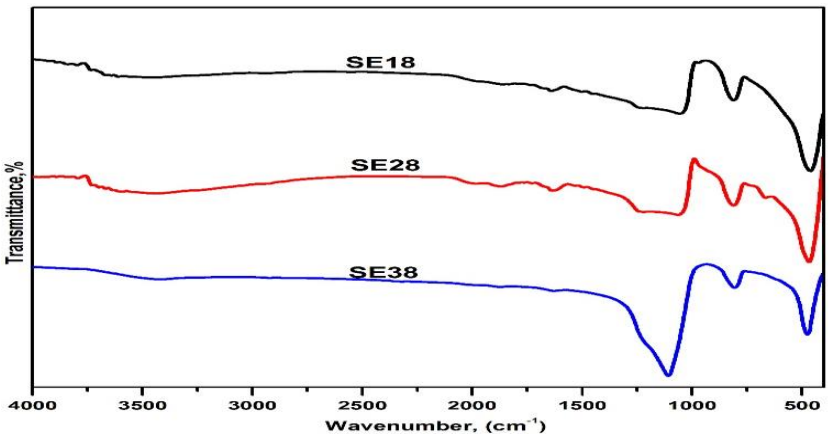

Fig (3): FTIR spectra of the calcined silicon oxide nanoparticles at 800 ºC for 4 h (SE18, SE28, and SE38 samples).

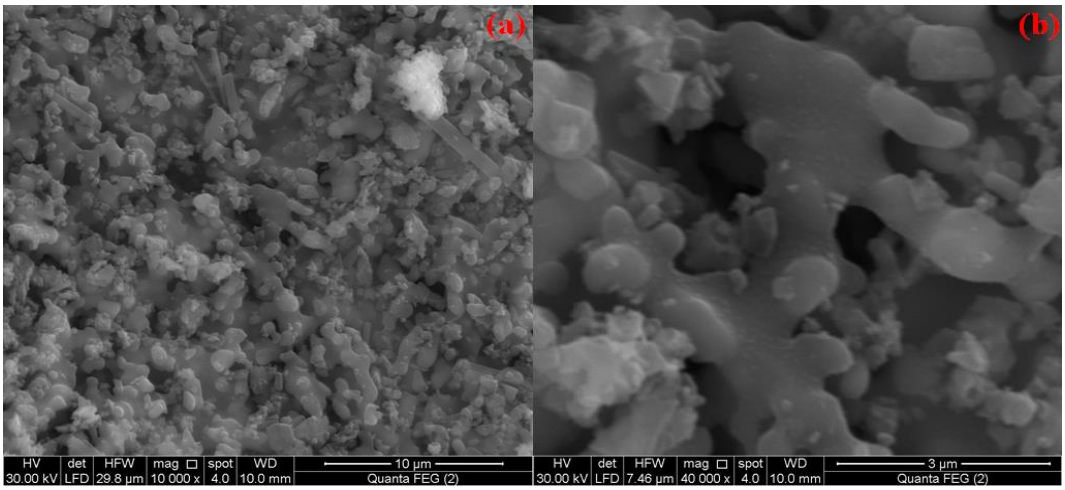

Fig (4): FE-SEM micrograph of the calcined silicon oxide (SE28 sample) at 800 ºC for 4 h.

3.2. Morphological studies

The morphology of the fabricated SiO_2 nanoparticles after the calcination at 800 ºC was studied using a field-emission scanning electron microscope (FE-SEM), as displayed in Figure (4). The FE-SEM micrograph of the silica sample exhibited that the product consisted of hard aggregation of two main different morphologies. The first type is the regular irregular shape and the average particle size was found to be 91 nm. The second type is the collection of the particle together in the form of tubes, with length 278 nm and diameter 34 nm.

4. Adsorption studies

The synthesized silicon oxide is used for the adsorption of congo red dye from aqueous media. Different factors that are required for the study of the removal of congo red dye: pH, adsorbent dose, time, and temperature. The removal of the congo red dye (20 mg/L) over 50 mg of the synthesized silicon oxide was studied over a wide range of pH from 5 to 10 as shown in Fig. 5(a)**.** After stirring for 24 h, the removal efficiency of the congo red dye reached its maximum which found to be 6.0 % (λ_{max} =498 nm at pH 6. The contact time of the adsorption of congo red (20 mg/L) over 0.05gm of silicon oxide was examined at pH 6, with stirring for 210 min. as shown in Fig. 5(b). The removal efficiency of the congo red dye was rapidly increased and it recorded 6 % at 40 min. The equilibrium condition was attained between 40-210 min and the removal percentage was found to be 6.2 %. The effect of initial concentrations on the removal of congo red dye is examined by using 50 mg of SiO_2 nanoparticles at pH 6 and initial concentrations in the range of 10 to 100 mg/L. After 50 min of stirring, the adsorption capacity of congo red dye was plotted with the initial concentrations as shown in Fig. 5(c)The adsorption capacity increased with the raising of the initial concentrations till 10mg/L and then, it became constant with 0.861 mg/g maximum adsorption capacity. The effect of adsorbent dose of SiO_2 on the removal of congo red dye was examined at the following conditions: was examined on the removal of congo red dye(20mg/g) at pH 6.0, The extracted data appeared that the removal of dye decreased with raising the amount of silicon oxide as shown in Fig. 5(d). The effect of temperature on the adsorption process of congo red dye was carried out at 30,35,40 and 45ºC, separately and the selected conditions: pH 6, 20 mg/L, and 40 min. The experimental study revealed that the removal decreased slowly by increasing temperature as shown in Fig.5(e). From the calculated data, the adsorption of congo red is an exothermic process.

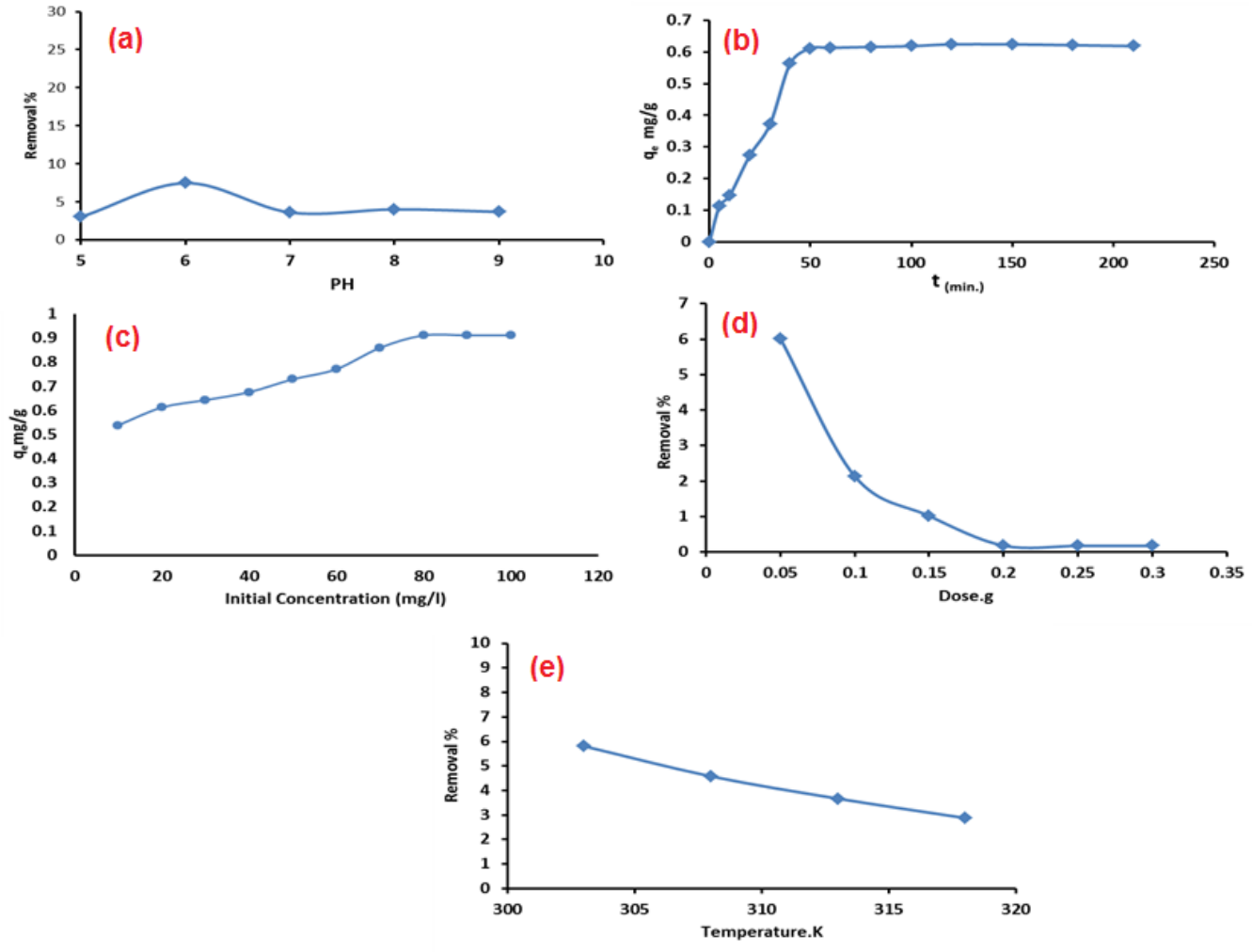

Figure (5): The experimental adsorption parameters for the removal of congo red dye over silicon oxide nanoparticles: (a) effect of pH, (b) effect of time, (c) effect of initial concentration, (d) effect of dose and (e) effect of temperature.

5. Adsorption Isotherms

Langmuir and Freundlich isotherm models were tested using 50 mg of silicon oxide (SE28 sample) and the determined experimental data like the following: initial concentration (10-100 mg/L), pH 6, 30 ^{o}C and 40 min. The selected isotherm models can be achieved using the following equations (2 and 3).

$$C_e/q_e = 1/(q_m K_L) + C_e/q_m \qquad (2)$$

$$\ln q_e = \ln K_F + (1/n)\ln C_e \qquad (3)$$

Where C_e, q_e, and q_m are the equilibrium concentration of dye (mg/L), amount of adsorbed dye at equilibrium, and the maximum capacity of adsorbed dye over silicon oxide (mg/g), respectively. K_L, K_F, and 1/n are Langmuir constant (L/mg), Frendlich constant (mg/g), and the heterogeneity factor, respectively. The essential characteristics of Langmuir isotherm can be expressed by a dimensionless constant called equilibrium parameter R_L, defined as:

$$R_L = \frac{1}{1 + bC_0} \qquad (4)$$

Where b is the Langmuir constant and C_0 is the initial dye concentration (mg/L), R_L value indicates the adsorption nature to be either unfavorable if $R_L > 1$, linear if $R_L = 1$, favorable if $0 < R_L < 1$ and irreversible if $R_L = 0$

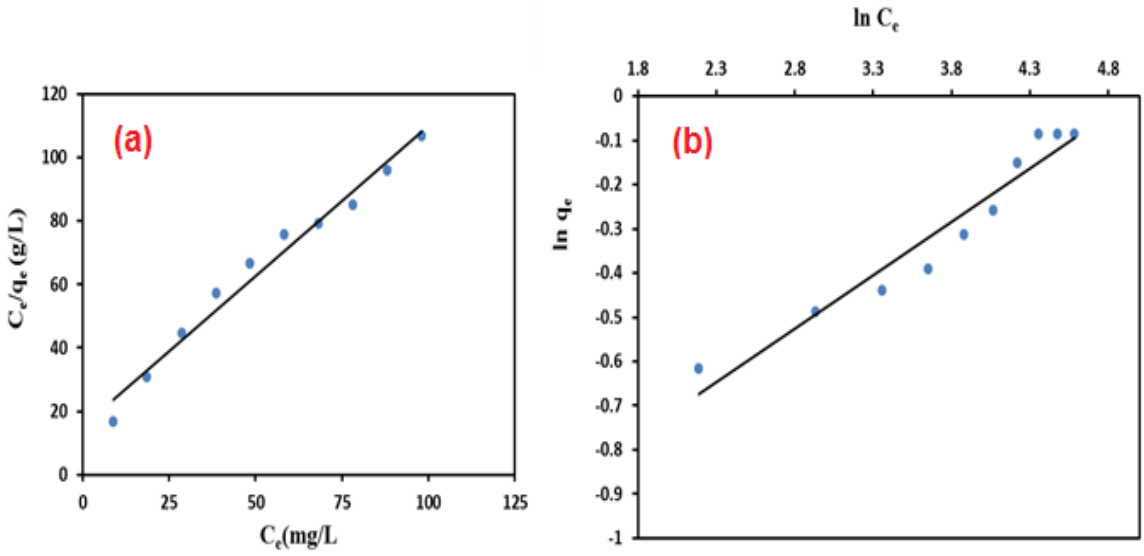

Fig (6) Langmuir (a) and Freundlich (b) isotherm models for the removal of congo red dye over silicon oxide nanoparticles,(SE28 sample)

Table 2 The extracted parameters of the applied isotherms for removal of congo red dye over silicon oxide nanoparticles.

Adsorption isotherm	Parameter	Values
Langmuir parameters	K_L (L/mg)	0.0627
	$q_{m\,(cal)}$ (mg/g)	1.054407
	R_L	0.1375 - 0.6164
	R^2	0.9773
	$q_{m\,(exp)}$ (mg/g)	0.861727
Freundlich parameters	K_F (L/mg)	0.06256
	$q_{m\,(cal)}$ (mg/g)	0.80727
	K_F	1.2037
	R^2	0.9355
	$q_{m\,(exp)}$ (mg/g)	0.860727

Figure (6) Displayed Langmuir and Freundlich isotherm models for the removal of congo red dye over silicon oxide nanoparticles (SE28 sample). Table 2 are outlined the extracted factors from Langmuir and Freundlich isotherm. From the R^2 values, Langmuir isotherm model is better fitting than the Freundlich isotherm. Besides, the estimated adsorption capacity from Langmuir isotherm was estimated to be (1.15 mg/g), which are approached from the experimental value (1.0544mg/g). From Table (2), R_L values show that the adsorption of congo red dye over silicon oxide nanoparticles is a favorable process.

6. Kinetic studies

Pseudo first order and pseudo-second-order reaction models are used for investigation of the rate of the removal of congo red dye over the fabricated silicon oxide (SE28 sample) as shown in the following equations(4 and 5).

$$\log(q_e - q_t) = \log q_e - \frac{K_1}{2.303}\, t \qquad (4)$$

$$\frac{t}{q_t} = \frac{1}{K_2 {q_e}^2} + \frac{t}{q_e} \qquad (5)$$

Where q_e and q_t are the quantities of adsorbed dye (mg/g) at equilibrium and time, K_1 (min^{-1}) and k_2 (g/mg/min) are constants of pseudo first and pseudo-second-order respectively figure 7 shows Pseudo first order and pseudo-second-order models for the removal of congo red dye over the synthesized silica (SE28 sample). Kinetic parameters were listed in Table 3 for the adsorption of congo red dye over the synthesized silicon oxide adsorbent. According to the correlation coefficients R^2, a pseudo-second-order was acceptable than pseudo-first-

order kinetic models. Depending on the extracted data, the adsorption capacity value (0.80727 mg/g) calculated from the pseudo-second-order kinetic model was near to the experimental value (0.86072 mg/g) for the removal of congo red dye over silicon oxide adsorbent. These previous results suggested that the pseudo-second-order adsorption can be applied.

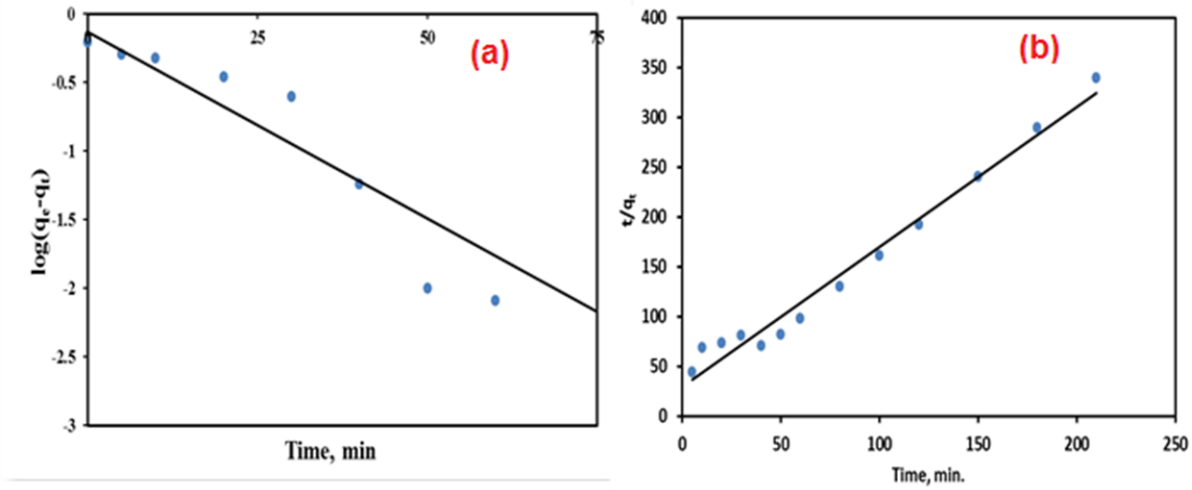

Fig (7) Pseudo-first-order model (a), pseudo-second-order model (b), for removal of the congo red dye using silicon oxide nanoparticles (SE28 sample).

Table 3
Kinetic parameters for adsorption of congo red dye over the synthesized silicon oxide adsorbent

Kinetic model	Parameter	Values
Pseudo first order	$K_1(min^{-1})$	0.062485
	$q_{m\,(cal)}$ (mg/g)	0.735047
	R^2	0.9209
	$q_{m\,(exp)}$ (mg/g)	0.62
Pseudo second order	K_2 (g/mg.min)	0. 066137
	$q_{m\,(cal)}$ (mg/g)	0.711613
	R^2	0.9783
	$q_{m\,(exp)}$ (mg/g)	0.62

7. Thermodynamic studies

Thermodynamic parameters (entropy change (ΔS^o), enthalpy change (ΔH^o), and free energy change (ΔG^o)) are related by Van't Hoff equation:(6,7 and 8) as the following:

$$\ln K_d = \frac{\Delta S^\circ}{R} - \frac{\Delta H^\circ}{RT} \qquad (6)$$

$$\Delta G^\circ = \Delta H^\circ - T\Delta S^\circ \qquad (7)$$

$$K_d = Q_e/C_e \qquad (8)$$

Where K_d is the Equilibrium constant, q_e is the adsorbent equilibrium concentration (mg/L), T in Kelvin and R is the gas constant. Plotting ln K_d against 1/T gives a straight line with slope and intercept equal to [$-\Delta H^o/R$] and [$\Delta S^o/R$], respectively. Thermodynamic parameters are determined and listed in Table 4.

The value of ΔH^o is lower than 40 KJ/mol, so the removal of congo red dye using silicon oxide nanoparticles indicated that the adsorption process was exothermic and physisorption process. The negative value of entropy change (ΔSo) corresponds to a decrease in the degree of freedom of the adsorbed species of removal congo red dye using silicon oxide. The positive values of ΔGo revealed that the separation process is

nonspontaneous. Additionally, the increase of ΔGo values with the raising of of congo red dye using silicon oxide is unfavorable at

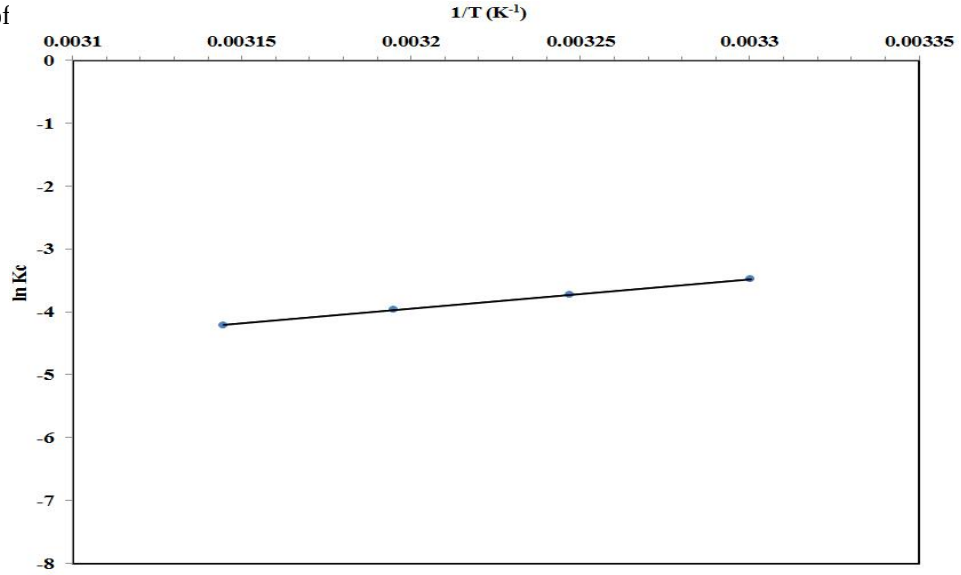

Fig (8) Van't Hoff plot for the adsorption of congo red dye on silicon oxide nanoparticles (SE28 sample).

Table 4

Thermodynamic data for adsorption of congo red dye over the synthesized silicon oxide adsorbent

Sample	T, (ºK)	ln K_c	ΔGº (KJ/mol)	ΔHº (KJ/mol)	ΔSº (KJ/mol)
SE28	303	-3.479017	8.7595	-38.93	- 0.1574
	308	-3.730098	9.5466		
	313	-3.961460	10.333		
	318	-4.212152	11.120		

5. Conclusions

Silica nanoparticles were fabricated by Sol-gel auto-combustion synthesis method followed by the calcination at 800 ºC for 4 h. The obtained sample was characterized by different tools such as XRD, FT-IR, and FE-SEM. The XRD pattern of calcined silicon showed that the characte6+ristic lines of the cristobalite phase of silicon oxide with an average crystallite size of 3-7.5 nm. The characteristic FTIR absorption peaks at 468, 665, 811, and 1064 cm^{-1} are attributed to Si-O, Si-O-Si stretching vibration modes of SiO_2[8]. The FE-SEM photograph displayed that the calcined silica nanoparticles show the spherical shapes with hard agglomeration and the average particle size in the range of 91 nm. It was found that the reaction rate of adsorption of congo red dye was obeyed pseudo-second-order. The adsorption process of congo red dye over silica nanoparticles can be fitted Langmuir isotherm model. The calculated thermodynamic factors (ΔGº, ΔHº and ΔS) exhibit that the adsorption process of congo red dye on silicon oxide was exothermic, so the adsorption is unfavorable at high temperatures.

Acknowledgments

The authors express their thanks to Benha University, Benha, Egypt for support of the current research.

References

[1] A.B. Corradi, F. Bondioli, A.M. Ferrari, B. Focher, C. Leonelli, Synthesis of silica nanoparticles in a continuous-flow microwave reactor, Powder Technol., Vol.(167), PP.45-48, 2006.

[2] I.A. Rahman, V. Padavettan, Synthesis of silica nanoparticles by sol-gel: size-dependent properties, surface modification, and applications in silica-polymer nanocomposites—a review, J. Nanomater., Vol.(2012), PP.1-15, 2012.

[3] A. Esmaeili-Bafghi-Karimabad, L. Nejati-Moghadam, M. Salavati-Niasari, S. Bagheri, Synthesis of SiO2

Nanocrystals by Two Approaches and Their Application in Photocatalytic Degradation and Flame Retardant Polymeric Nanocomposite, J. Inorg. Organomet. Polym Mater., Vol.(29),PP.378-389, 2019.
[4] D. Gong, X. Hui, Z. Guo, X. Zheng, The synthesis of PEI core@ silica shell nanoparticles and its application for sensitive electrochemical detecting mi-RNA, Talanta, Vol.(198),PP.534-541, 2019.
[5] X. Su, Y. Tang, Y. Li, Z. Wang, J. Tao, K. Chen, Y. Liu, J. Wu, D. Wang, Z. Teng, Facile Synthesis of Monodisperse Hollow Mesoporous Organosilica/Silica Nanospheres by an in Situ Dissolution and Reassembly Approach, ACS Appl. Mater. Interfaces, Vol.(11),PP.12063-12069, 2019.
[6] G. Patonay, M. Henary, G. Chapman, W. Abdelwahab, Surface modified fluorescent silica nanoparticles and their applications (Conference Presentation), in: Reporters, Markers, Dyes, Nanoparticles, and Molecular Probes for Biomedical Applications XI, International Society for Optics and Photonics, Vol.(10893),PP.1-7, 2019.
[7] M. Khoeini, A. Najafi, H. Rastegar, M. Amani, Improvement of hollow mesoporous silica nanoparticles synthesis by hard-templating method via CTAB surfactant, Ceram. Int., Vol.(45),PP.12700-12707, 2019.
[8] M.Y. Nassar, I.S. Ahmed, M.A. Raya, A facile and tunable approach for synthesis of pure silica nanostructures from rice husk for the removal of ciprofloxacin drug from polluted aqueous solutions, J. Mol. Liq., Vol.(282),PP.251-263, 2019.
[9] D. Gößl, H. Singer, H.-Y. Chiu, A. Schmidt, M. Lichtnecker, H. Engelke, T. Bein, Highly active enzymes immobilized in large pore colloidal mesoporous silica nanoparticles, New J. Chem., Vol.(43),PP.1671-1680, 2019.
[10] W. Zhang, N. Zheng, L. Chen, L. Xie, M. Cui, S. Li, L. Xu, Effect of Shape on Mesoporous Silica Nanoparticles for Oral Delivery of Indomethacin, Pharmaceutics, Vol.(11),PP.1-13, 2019.
[11] H. Abe, I. Abe, K. Sato, M. Naito, Dry powder processing of fibrous fumed silica compacts for thermal insulation, J. Am. Ceram. Soc., Vol.(88),PP.1359-1361, 2005.
[12] Y. Luo, Y. Jiang, J. Feng, J. Feng, Synthesis of white cement bonded porous fumed silica-based composite for thermal insulation with low thermal conductivity via a facile cast-in-place approach, Constr. Build. Mater., Vol.(206),PP.620-629, 2019.
[13] C. Lee, H. Na, Y. Jeon, H.J. Hwang, H.-J. Kim, I. Mochida, S.-H. Yoon, J.-I. Park, Y.-G. Shul, Poly (ether imide) nanofibrous web composite membrane with SiO2/heteropolyacid ionomer for durable and high-temperature polymer electrolyte membrane (PEM) fuel cells, J. Ind. Eng. Chem., Vol.(74),PP.7-13, 2019.
[14] S. Yoon, T. Ryu, K. Kim, S.S. Chandra, F. Ahmed, H. Yang, S. Lee, J. Kim, W. Kim, Synthesis of Sulfonation Poly (N-propylsulfonicacid isatin biphenylene) for Polymer Electrolyte Membrane Fuel Cell Containing SiO2 Nanocomposite Membrane, J. Nanosci. Nanotechnol., Vol.(19),PP.1562-1566, 2019.
[15] Y. Kotolevich, O. Martynyuk, S. Martínez-González, H. Tiznado, A. Pestryakov, M.A. Borja, V.C. Corberán, N. Bogdanchikova, Novel route of synthesis of ultra-small Au nanoparticles on SiO2 supports, Fuel, Vol.(236),PP. 589-597, 2019.
[16] K. Durairaj, P. Senthilkumar, P. Velmurugan, K. Dhamodaran, K. Kadirvelu, S. Kumaran, Sol-gel mediated synthesis of silica nanoparticle from Bambusa vulgaris leaves and its environmental applications: kinetics and isotherms studies, J. Sol-Gel Sci. Technol., Vol.(90),PP. 653-664 2019.
[17] S. Gunatilake, Methods of removing heavy metals from industrial wastewater, Methods, 1 (2015) 14.
[18] M. Maiti, M. Sarkar, S. Xu, S. Das, D. Adak, S. Maiti, Application of silica nanoparticles to develop faujasite nanocomposite for heavy metal and carcinogenic dye degradation, Environ. Prog. Sustain. Energy, Vol.(38),PP. S15-S23 2019.
[19] S.R. Almeida, C. Elicker, B.M. Vieira, T.H. Cabral, A.F. Silva, P.J. Sanches Filho, C.W. Raubach, C.A. Hartwig, M.F. Mesko, M.L. Moreira, Black SiO2 nanoparticles obtained by pyrolysis of rice husk, Dyes and Pigments, Vol.(164),PP.272-278, 2019.
[20] G. Yang, Q. Guo, D. Yang, P. Peng, J. Li, Disperse ultrafine amorphous SiO2 nanoparticles synthesized via precipitation and calcination, Colloids Surf., A, Vol.(568),PP.445-454, 2019.
[21] M.E. Mahmoud, S.S. Hassan, A.H. Kamel, M.I. Elserw, Development of microwave-assisted functionalized nanosilicas for instantaneous removal of heavy metals, Powder Technol., Vol.(326), PP.454-466, 2018.
[22] S. Tighadouini, S. Radi, M. Anannaz, M. Bacquet, S. Degoutin, M. Tillard, D. Eddike, H. Amhamdi, Y. Garcia, Engineering β-ketoenol structure functionality in hybrid silica as excellent adsorbent material for removal of heavy metals from water, New J. Chem., Vol.(42), PP. 13229-13240, 2018.
[23] H. Vojoudi, A. Badiei, S. Bahar, G.M. Ziarani, F. Faridbod, M.R. Ganjali, A new nano-sorbent for fast and efficient removal of heavy metals from aqueous solutions based on modification of magnetic mesoporous silica nanospheres, J. Magn. Magn. Mater., Vol.(441), PP.193-203, 2017.
[24] W. Jia, H. Xu, Q. Yang, S. Ren, J. Wang, Synthesis of anionic gemini surfactant-templated mesoporous silica nanoparticles and its adsorption application for Pb2+, J. Dispersion Sci. Technol., Vol.(40), PP.1664-1674, 2019.

[25] P. Jiang, L. Zhang, J. Ge, G. Zhang, H. Pei, Phase inversion of emulsions stabilized by lipophilic surfactants and SiO2 nanoparticles, Colloids Surf., A, Vol.(562), PP. 42-53, 2019.
[26] A. Alighardashi, M.J. Mehrani, A.M. Ramezanianpour, Pervious concrete reactive barrier containing nano-silica for nitrate removal from contaminated water, Environ. Sci. Pollut. Res., Vol.(25), PP.29481-29492, 2018.
[27] I. Ahmed, H. Dessouki, A. Ali, Synthesis and characterization of new nano-particles as blue ceramic pigment, Spectrochim. Acta, Part A , Vol.(71), PP.616-620, 2008.
[28] A. Ali, E. El Fadaly, I. Ahmed, Near-infrared reflecting blue inorganic nano-pigment based on cobalt aluminate spinel via combustion synthesis method, Dyes and Pigments, Vol.(158), PP.451-462, 2018.
[29] A.A. Ali, M.R. Allazov, T.M. Ilyasli, Synthesis and characterization of magnesium aluminates spinel via combustion method using malonic acid dihydrazide as fuel, Casp. J. Appl. Sci. Res., Vol.(2), PP.85-90, 2013.
[30] K. Patil, Chemistry of nanocrystalline oxide materials: combustion synthesis, properties and applications, World Scientific,PP.42-58, 2008.
[31] H.C. Yi, J. Moore, Self-propagating high-temperature (combustion) synthesis (SHS) of powder-compacted materials, J. Mater. Sci., Vol.(25), PP.1159-1168, 1990.